JOURNAL OF COMPUTATIONAL PHYSICS 75, 300–313 (1988)

Hyperviscosity for Compressible Flows Using Spectral Methods

T. PASSOT AND A. POUQUET

Observatoire de Nice, B. P. 139, 06003 Nice Cedex, France

Received July 15, 1986; revised February 5, 1987

We describe a method for direct numerical simulations of highly turbulent compressible flows which permits an enhancement of the Reynolds number. A modification of the dissipative terms of the hydrodynamical equations is introduced in a way that preserves, by construction, the thermodynamic laws of the dissipation functions. At constant cost, the simulated Reynolds numbers can be two orders of magnitude larger than with the standard Navier–Stokes equation. We also compare our method with the artifical viscosity scheme customary to spectral methods, namely using high powers of the Laplacian, and show that results are improved, in our case, leaving out spurious oscillations near the shock, in particular.

1. INTRODUCTION

Numerical simulations of flows, in the spirit of experimentation, are only in their infancy because of the severe lack of resolution of present-day supercomputers. Among the many available numerical schemes, spectral ones are known for their precision, as long as the flow remains smooth. Several compressible dissipative flows in the turbulent regime have been simulated with spectral methods, both in two dimensions [1–3] and in three dimensions [4], though at substantially lower Reynolds number in the latter case. No Gibbs phenomenon occurs in these simulations because shocks are smoothed out by adequate viscosity, spreading them on five to eight grid points. The spectral precision is thus preserved down to the dissipative scale: structures observed on derivative fields, such as vorticity sheets and, in magnetohydrodynamics, current sheets, are adequately resolved. This is particularly important when dealing with instabilities of the diffusive type, for example, the resistivity-dependent tearing mode of current sheets. It should be noted that in MHD, one can simulate flows for magnetic Reynolds numbers that are not attainable in the laboratory (except, marginally, in industrial equipment such as the liquid sodium of metal-cooled breeder reactors) and yet are essential in the understanding of the generation of large scale magnetic fields that are observed in many cosmic objects. However, when dealing with various aerodynamical or astrophysical problems in which the fluctuating Mach number is above unity and the Reynolds number is very large [5], the numerical wind-tunnel approach proves

0021-9991/88 $3.00

insufficient. In such cases, one resorts to a modeling of the flow, for which a large spectrum of possibilities exists. One seeks to obtain not only a correct treatment of the behavior of the large-scale energy-containing eddies, but also an adequate representation of the structures occurring in physical space down to some intermediate scale as close as possible to the dissipation wavelength. In this context, large grids are still needed to resolve the small scales, and it is in the handling of dissipation that large Reynolds numbers become available. In this approach, one does not attempt to simulate the Euler equations with an artificial viscosity to smooth out the shocks [6, 7]. Rather, one tries to remain as close as possible to Navier Stokes flows, in order to preserve the adequate representation of non-local effects between widely separated scales, in particular. Indeed, the turbulent viscosity that represents the enhanced dissipation of energy due to the non-explicitly treated small scales is well known; however, in some cases, transport coefficients can be negative, leading to large-scale instabilities due to averaging effects over the small scale turbulence.

In spectral codes using Fourier decomposition, the Laplacian is diagonal and a very simple hyperviscosity law is to use powers of the Laplacian higher than unity. This technique has been studied in the mathematical context to prove global regularity of the thus-modified Navier–Stokes equations [8]. Its implementation on two-dimensional flows is well documented [9, 10] and in three-dimensional MHD it proved useful in studying the inverse transfer of magnetic helicity [9]. This method restricts the dissipation range to a small interval of wavenumbers, thus leaving more room for the inertial range in which nonlinear effects prevail. However, the associated dissipation function is not everywhere positive and, when applied to compressible flows, it leads to spurious oscillations in the shocks. This part is treated in Section 2. We present in Section 3 a systematic procedure to construct new dissipation functionals that remain positive by generalizing the Navier-Stokes constitutive laws to the nonlinear case. This method is tested numerically in Section 4 against high-resolution numerical experiments, and Section 5 is the Conclusion.

2. The Case of the Bi-Laplacian

We consider the compressible fluid equations for the density ρ, the momentum ρu (where u is the velocity) and the energy E:

$$\begin{aligned} \partial_t \rho + \nabla(\rho u) &= 0 \\ \partial_t \rho u + \nabla \cdot (P\mathbf{I} + \rho \mathbf{u}\mathbf{u}) &= \nabla \cdot \boldsymbol{\tau} \\ \partial_t E + \nabla((E+P)\,u) &= K\nabla^2 T + \nabla(\boldsymbol{\tau} \cdot u), \end{aligned} \tag{2.1}$$

where the usual formulation of the stress tensor (Navier–Stokes law) is

$$\boldsymbol{\tau} = \lambda(\operatorname{div} u)\,\mathbf{I} + 2\mu\mathbf{D} \tag{2.2}$$

with $D_{ij} = \frac{1}{2}(u_{i,j} + u_{j,i})$ being the deformation tensor and λ and μ the Lamé coefficients; $\mathbf{I}$ is the identity tensor and partial derivative in the j direction is denoted by j, in (2.1) P is the pressure (determined through, for example, the perfect gas law) and K is the thermal diffusion coefficient. When we restrict the problem to the one-dimensional case, we can write $\nabla(\boldsymbol{\tau}) = \mu_1 \Delta u$, which in Fourier space is simply

$$\widehat{\nabla \cdot \boldsymbol{\tau}} = -\mu_1 k^2 \hat{u}(k),$$

where $\hat{u}(k)$ is the Fourier transform of the velocity field $u(x)$ and where k is the wavenumber. The dissipation $\mu_1(\partial_x u)^2$ is proportional in Fourier space to k^2 and is more important in the small scales. When simulating turbulent flows with a finite number of Fourier modes, the coefficient μ_1 is so chosen as to ensure that the energy spectrum in the small scales drops off sufficiently fast without letting energy accumulate there. This poses a severe constraint on the Reynolds numbers than can be simulated without truncation error using the Navier–Stokes equation. This well-known problem can be circumvented by modifying the primitive equations in such a way as to concentrate dissipation to a smaller range of wavenumbers. In a spectral code using Fourier expansions for which the Laplacian operator is diagonal, a particularly simple choice of an hyperviscosity is to take a dissipation proportional to $k^{2\alpha}$ ($\alpha > 1$). With $\alpha = 2$, the form commonly used is thus

$$\widehat{\nabla \cdot \boldsymbol{\tau}} = -\mu_1' k^4 \hat{u}(k); \tag{2.3}$$

to adjust the new viscosity coefficient μ_1', one writes

$$\mu_1 k_{\max}^2 = C \mu_1' k_{\max}^4, \tag{2.4}$$

where $k_{\max}$ is the cut-off wavenumber and C a constant of order one to be adjusted empirically. We see that the relationship (2.4) implies that the enhancement of the Reynolds number in the large scales (corresponding to $k_{\min} = 1$) is of the order of $k_{\max}^{2(\alpha-1)}$ and is thus very effective. We should here mention that the relationship between local Reynolds number and scale varies with α; the condition (2.4) indicates that the local Reynolds number at the dissipation scale (close to $k_{\max}^{-1}$) is of order unity whatever the choice of α.

In real space, (2.3) implies that $\boldsymbol{\tau} = -\mu_1 \partial_{xxx}^3 u$. We can thus express the dissipation $d = \boldsymbol{\tau} : \mathbf{D}$ as

$$d = -\mu_1'(\partial_{xxx}^3 u) \cdot \partial_x u.$$

This expression is not everywhere positive, whereas the integrated dissipation $\int d\,dx = \int (\partial_{xx}^2 u)^2\,dx$ clearly is. We show the sketch of a triangular shock in Fig. 1a, of the dissipation d in Fig. 1b and of the result of a numerical simulation in the one-dimensional case in Fig. 1c using a spectral method [12] and the expression (2.3). We see that at the edges of the shock, energy is fed into the system instead of being removed, because of the oscillations of the dissipation d around zero. This explains

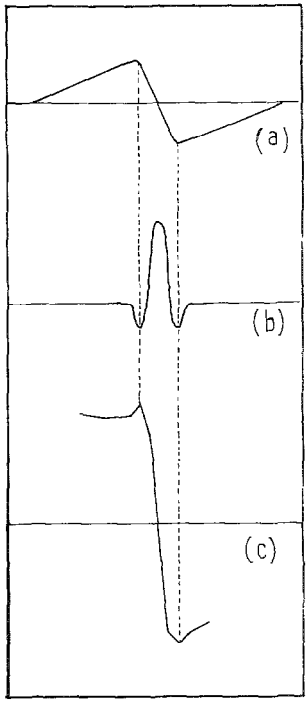

FIG. 1. Sketch of a triangular shock (a) and of the corresponding dissipation $d = -\mu(\partial^3_{xxx} u)\,\partial_x u$ (b); in (c), we plot the profile of a velocity jump computed numerically with the bi-Laplacian method. Note the oscillations when the dissipation d is negative.

the pre- and post-shock oscillations of the numerical simulation; they are not related to the Gibbs phenomenon, which would appear on top of it for values of μ'_1 smaller than that used in the computation reported here.

Although one could remove such oscillations with a proper filtering of the velocity field, another possibility is to find a pseudo-viscosity tensor which compels the dissipation to be everywhere positive. This is done in the next Section.

3. The Derivation of a High-Order Positive Dissipation Function

We want to find a natural way to generalize the Navier–Stokes law in order to have a dissipation proportional to k^4 (in Fourier space) in regions of sharp gradients, together with the positivity of the local dissipation in real space. This latter property, which holds for Navier–Stokes flows, is important when seeking to avoid spurious oscillations near the shock, as we have shown in Section 2. Instead of proceeding in an empirical way to derive a model of the small scales that are not treated explicitly in the computation, we propose to start from first principles

and retain this structural property of the Navier–Stokes equations which appears particularly important in the highly compressible case.

The Navier–Stokes laws may be derived from a pseudo-potential of dissipation $\varphi_2(\mathbf{D})$, where $\mathbf{D}$ is the deformation tensor. In this formulation, the stress tensor $\boldsymbol{\tau}$ is the gradient of the quadratic functional $\varphi_2(\mathbf{D})$. Note that φ_2 is, within an additive constant, the free energy which must be minimum at local thermodynamic equilibrium [13, 14]. This in turn implies that φ_2 is positive definite and convex. The dissipation is then

$$\boldsymbol{\tau} : \mathbf{D} = \frac{\delta \varphi_2(D_{ij})}{\delta D_{ij}} \cdot D_{ij} = 2\varphi_2(D_{ij}),$$

where the Einstein summation convention is employed and δ denotes functional derivative. The last part of the equality stems from the fact that φ_2 is a homogeneous polynomial of D_{ij} (Euler's theorem).

This constitutive law, relating $\boldsymbol{\tau}$ with $\mathbf{D}$, can be viewed as the linear first-order approximation of a more general expansion. We will thus consider a potential of dissipation which is a quartic homogeneous functional of $\mathbf{D}$. The general form of this potential $\varphi_4(\mathbf{D})$, assuming isotropy, can be easily expressed from the three invariants of $\mathbf{D}$, namely:

$$I_1 = D_{ii}, \tag{3.1}$$

$$I_2 = D_{ij} D_{ij}, \tag{3.2}$$

$$I_3 = D_{ij} D_{jk} D_{ki}. \tag{3.3}$$

All other invariants of higher order are a combination of these three. We recall here the more general form of the quadratic functional $\varphi_2(\mathbf{D})$,

$$\varphi_2(\mathbf{D}) = \tfrac{1}{2}(\lambda I_1^2 + 2\mu I_2),$$

which gives for $\boldsymbol{\tau}$ the usual expression,

$$\tau_{ij} = \lambda D_{kk} \delta_{ij} + 2\mu D_{ij},$$

with the positivity of $\varphi_2(\mathbf{D})$ obtaining when $\mu > 0$ and $\lambda \geqslant \frac{2}{3}\mu$. In the quartic case one writes

$$\varphi_4(\mathbf{D}) = \alpha_1 I_1^4 + \alpha_2 I_1^2 I_2 + \alpha_3 I_2^2 + \alpha_4 I_1 I_3,$$

which gives for $\boldsymbol{\tau} = \nabla \varphi_4(\mathbf{D})$:

$$\begin{aligned} \tau_{ij} = {} & [4\alpha_1 I_1^3 + 2\alpha_2 I_1 I_2 + \alpha_4 I_3]\, \delta_{ij} \\ & + [2\alpha_2 I_1^2 + 4\alpha_3 I_2]\, D_{ij} + 3\alpha_4 I_1 D_{ik} D_{kj}. \end{aligned} \tag{3.4}$$

The coefficients α_i appearing in the above expression are not entirely arbitrary; indeed, there are constraints on them so that the dissipation $\boldsymbol{\tau} : \mathbf{D} = 4\varphi_4(\mathbf{D})$ is positive for all values of D_{ij}. We exhibit such constraints for two cases. For example, for incompressible flows, $I_1 = 0$ and $\varphi_4(\mathbf{D}) = \alpha_3 I^2$. Since $I_2 > 0$, we must have $\alpha_3 > 0$. On the other hand, for tensors of the form $\mathbf{D} \propto \mathbf{I}$, we have

$$I_2 = \tfrac{1}{3} I_1^2,$$
$$I_3 = \tfrac{1}{9} I_1^3,$$

and we find that $\alpha_1 + \frac{1}{3}\alpha_2 + \frac{1}{9}\alpha_3 + \frac{1}{9}\alpha_4 \geqslant 0$.

Note that this case of spherical tensors corresponds to uniform compression. The expression for τ_{ij} given above is rather complicated. Having in mind numerical applications, we shall therefore set $\alpha_4 = 0$, which eliminates the term in (3.4) most cumbersome to compute. Furthermore, in the two-dimensional problem, the following relation holds:

$$I_3 = \tfrac{3}{2}(I_2 - I_1^2)\, I_1,$$

and the above simplification becomes rigorous.

Seeking to reduce further the number of coefficients α_i, we can use particular forms of the stress tensor τ_{ij} depending only on one parameter μ. For example, by letting $\alpha_1 = \frac{1}{18}\mu$, $\alpha_2 = -\frac{1}{3}\mu$, $\alpha_3 = \frac{1}{2}\mu$, and $\alpha_4 = 0$ in (3.4), one obtains:

$$\tau_{ij} = \mu[I_2 - \tfrac{1}{3} I_1^2][-\tfrac{2}{3} I_1 \delta_{ij} + 2D_{ij}]. \tag{3.5}$$

This can be interpreted as the usual formula for τ_{ij} (when bulk viscosity is neglected) in which the viscosity coefficient is dependent upon the fluid deformations.

Another one parameter-dependent form for τ_{ij} is obtained by simply setting $\alpha_2 = 0$ and $\alpha_1 = \alpha_3 = \frac{1}{4}\mu$. In that case,

$$\tau_{ij} = \mu[I_1^3 \delta_{ij} + I_2 D_{ij}]. \tag{3.6}$$

In the following, we will only consider the formulation (3.5), which is closer to the usual Navier–Stokes law.

We would like to point out that the internal stress tensor derives from a potential: this fact restricts the possible expressions for $\boldsymbol{\tau}$. Recall indeed that the Lamé coefficients λ and μ usually depend only on temperature. An a priori natural generalization may be to make them also velocity dependent. However, an arbitrary expression in terms of the invariants (3.1)–(3.3) does not ensure that $\boldsymbol{\tau}$ will derive from a potential and thus will not satisfy general thermodynamical constraints [13, 14]. When, for numerical purposes one looks for simplified expressions of the stress tensor, one ought to start from (3.4).

It is in principle possible to generalize this approach to higher order potentials, but we make no attempt at that in this paper and now turn to numerical experimentation using for the stress tensor the expression (3.5).

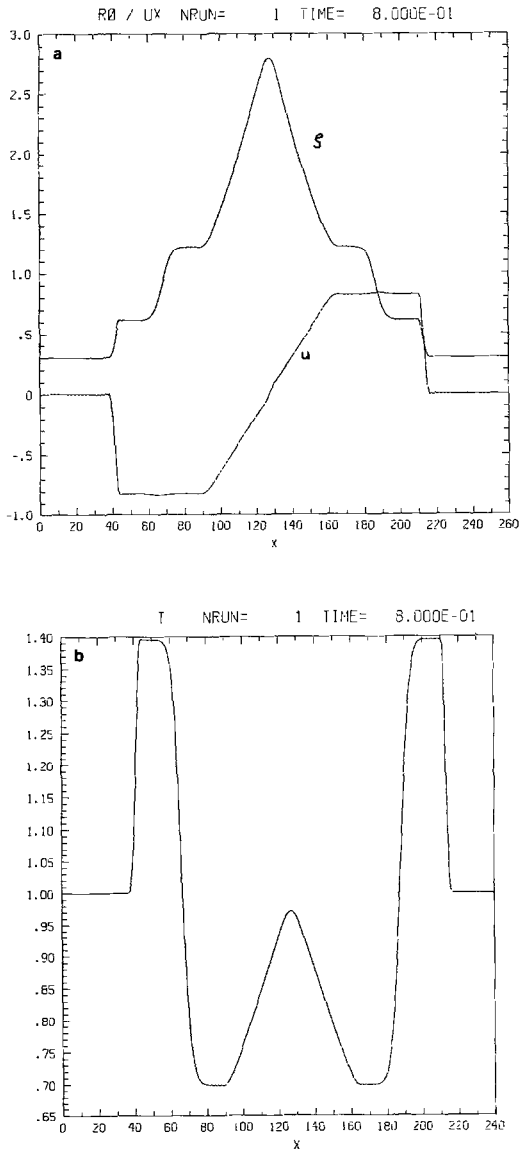

FIG. 2. Shock tube simulation for $\gamma = 1.4$ on a 256 points grid using $\tau = \mu(\partial_x u)^2 \partial_x u$ with $\mu = 10^{-4}$ and a Prandtl number of 0.05: (a) density and velocity profiles; (b) temperature.

4. Numerical Experiments

The formulae for the stress tensor derived in the previous section poses no particular numerical problem. Here we wish to test the validity of the method and, in particular, to compare it against actual flow computations using the primitive Navier–Stokes equations.

4.1. *The One-Dimensional Shock Tube Problem*

We begin with a classical problem, that of the shock tube. Initially, the density jump is 10, the temperature is constant, and the velocity is zero. The computation is made with a pseudo-spectral code described in [3], on a uniform grid of 256 points. A brief description of the numerical method is given in the Appendix. We use $\tau_{ij} = \mu(\partial_x u)^2 \cdot \partial_x u$ with $\mu = 10^{-4}$. The Rankine–Hugoniot relations are verified to within 0.5%. In fact, the results are indistinguishable from those reported in [3] in the case of the Navier–Stokes equations (see Fig. 2). The velocity jump is correctly computed. On the other hand, we were led to use a nonzero thermal diffusivity in order to treat correctly the temperature jump at the contact discontinuity. This discontinuity thus extends on two more points than the shocks do.

The hyperviscosity method described in this paper pertains to the class of explicit artificial viscosity [6] in which shocks are spread on at least four points. With methods of implicit viscosity, in which one integrates the Euler equations and imposes jump conditions, shocks can be restricted to extend on 2 or 3 points by construction. In our case, shocks still have to extend on enough points that Gibbs phenomenon does not occur, but we have not altered the physical state outside the shock, nor the speed of the shock.

4.2. *Two-Dimensional Homogeneous Flows*

We now show that the hyperviscosity method described in Section 3 permits us to reproduce results obtained with the Navier–Stokes equations at a substantially lower cost. As we shall see below, not only large-scale (integrated) quantities are recovered, but also intermediate temporal and spatial scales.

The Navier–Stokes run was described in [3] and was done on a 256×256 grid. We have performed a computation on a 64×64 grid using for the dissipation the expression (3.5); we adjust the value of the coefficient μ so that, for short times, the temporal evolution of the large scales, measured, for example, through the temporal evolution of the kinetic energy, is identical to that of the Navier–Stokes run. In Fig. 3, we show the result of such a comparison on the evolution of the fluctuating Mach number Ma and on the ratio $\mathcal{X}$ of the compressible energy to the kinetic energy. The solid line represents the Navier–Stokes run (in which the viscosity is equal to 10^{-2}) and the dotted line, when visible, corresponds to the hyperviscosity run, with $\mu = 2.5 \times 10^{-3}$. The remarkable feature of Fig. 3 is that these overall quantities are reproduced in a detailed manner, with plateaux in the Mach number of the same length and amplitude in both cases. A further comparison has been performed for the same parameters using the bi-Laplacian method. All three runs lead to

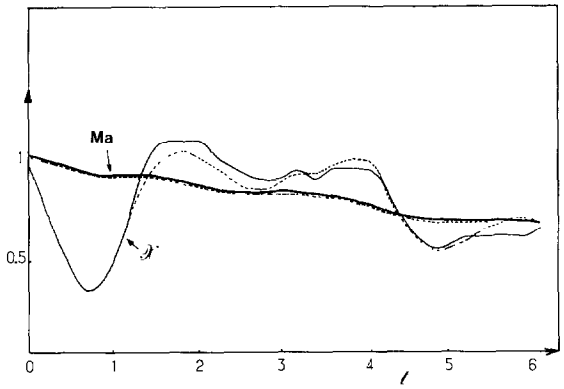

FIG. 3. Temporal evolution of the fluctuating Mach number Ma and of the ratio of compressible to kinetic energy $\mathscr{X}$ for both the 256×256 points Navier–Stokes run (solid line) and the 64×64 points hyperviscosity run (dashed line).

the same behavior, to within a few percent, in the large scales. However, as noted before, more oscillations are obtained in the velocity, entropy, and density variables when using the bi-Laplacian, because of the development of strong shocks. Highly compressible flows thus seem more sensitive than incompressible ones to proper treatment of dissipation.

When investigating the detailed spatial structures of the flow, one requires more resolution to be able to see details down to a given scale (as measured in units of the computational box, here $L = 2\pi$). Indeed, we show in Fig. 4a the density field in the Navier Stokes run. The field obtained with the 64×64 hyperviscosity computation has the same overall appearance (not shown). In particular, the strong collision of shocks in the upper left-hand corner is at the same position, and shocks are in both cases roughly five points wide; taking the length of the box to be constant, in the smaller resolution run, shocks thus appear wider (roughly by a factor $256/64 = 4$). However, if we now look at small scales, for example, displaying the vorticity, the features visible on Fig. 5a for the Navier–Stokes run are not easily identifiable in the 64×64 run. We therefore upgraded the resolution to 128×128, using a value of $\mu = 10^{-3}$. We show in Figs. 4b and 5b the density and the vorticity of this run at the same time. The overall aspect of the density field is the same, with individual values of local high and low differing by less than 6% (contour intervals are equal in both cases to 0.8). In the case of the vorticity, the Navier–Stokes run is dominated by the vortex-pair production at the place where two strong shocks collide (upper left-hand corner) with a local intensity of ± 12. These vortices also appear in the hyperviscosity run, but at a much lower intensity and, in fact, they do not dominate the flow. Note that the contour interval in Fig. 5a is 1.0 and in Fig. 5b, it is 0.3. However, the large-scale vortices, elongated approximately in the vertical direction, are reproduced fairly well in both runs, with local peaks and troughs of similar height. The reason why the local vorticity production of the

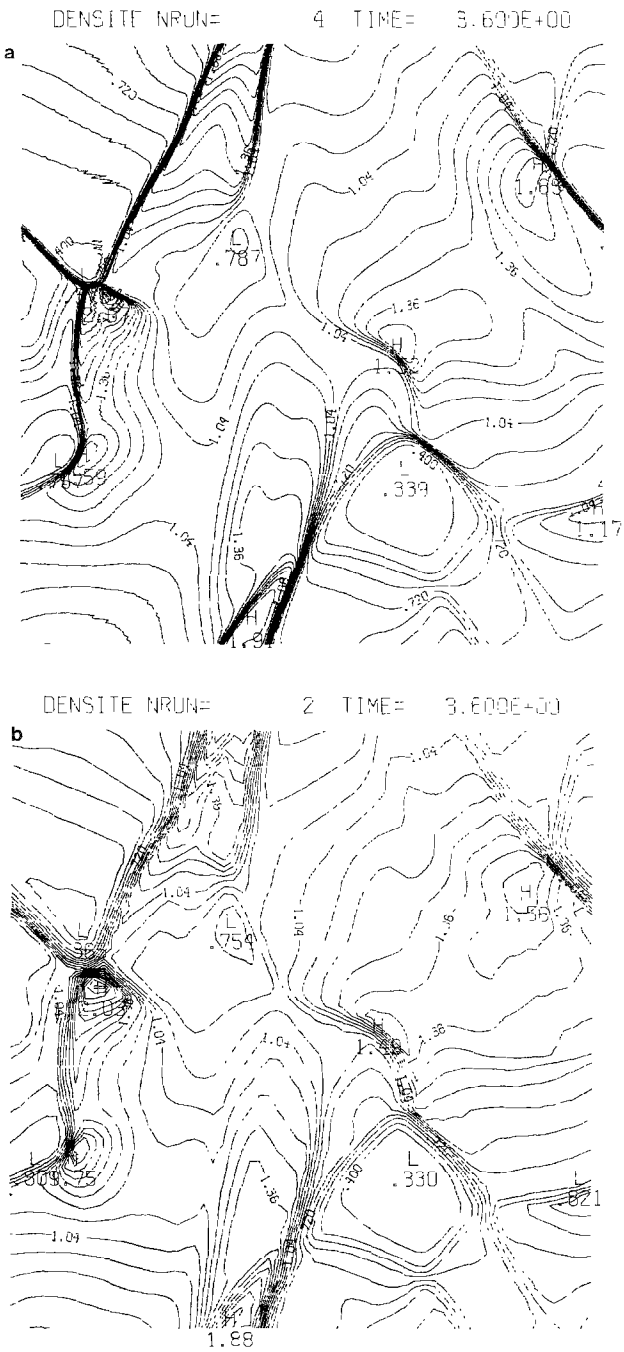

FIG. 4. Density field for the 256×256 points Navier–Stokes run (a) and the 128×128 points hyperviscosity run (b).

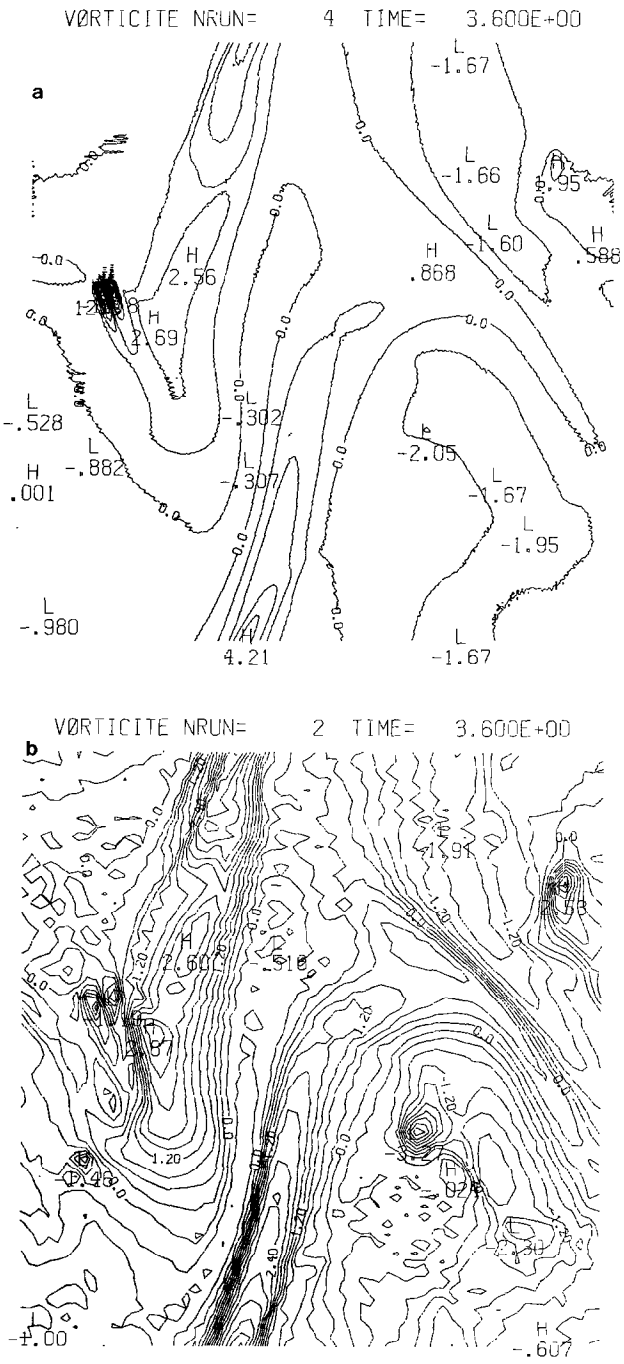

FIG. 5. Vorticity field for the two runs of Fig. 4.

Navier–Stokes run is not well reproduced here is simply due to the fact that the scale at which these vortex pairs appear is dependent upon the local geometry and thermodynamics of the shock collision [3]. In the Navier–Stokes run, they appear at a scale that is far enough from the dissipative range to be able to survive. In the hyperviscosity run, on the other hand, the vortex pair is formed at a scale which is roughly twice that of the width of the shock, and thus cannot grow because the rapid dissipation is overwhelming.

We would like to make two final remarks. First of all, the functional form of the dissipation tensor we use is nonlinear. Other forms of eddy viscosities have been proposed for incompressible flows that are nonlinear. For example, the one given by Smagorinsky [15], which is widely used in the context of meteorology, stems from one-point closures of turbulence in the spirit of the $K-\varepsilon$ models. The extension of such models to compressible flows is a matter of current research [16].

The nonlinearity of the dissipative scheme may lead to spurious energy spectra when using too small a value of the hyperviscosity coefficient. In the case of a pure Laplacian, energy then piles up in the small scales and the computation blows up reasonably rapidly. Here, a sharp increase in the small scales may occur instead of an exponential fall-off. Such equilibria should be discarded on general energetic principles.

Finally, let us point out that we did not encounter any special problem of numerical stability in simulating the equations with the hyperviscosity described here. This is probably related to the fact that the dissipation has the correct properties of convexity and positivity. Indeed, the argument of convexity is sufficient [13] to ensure the thermodynamical stability.

5. Conclusion

We have derived in this paper a method of numerical modeling of high Reynolds number flows starting from first principles. This approach leads naturally to positive dissipation functionals, thus avoiding the defect of hyperviscosity methods currently used in numerical simulations employing spectral (or pseudo-spectral) techniques. We have compared these modeled flows directly with actual experimental simulations of Navier–Stokes flows performed at the highest resolution available on a CRAY 1. This comparison is done in the two-dimensional homogeneous case for a perfect gas. We show that the essential features of the flow are preserved. In the large scale, we reproduce the temporal evolution of several variables, such as the r.m.s. Mach number or the mechanical energy at a cost roughly two orders of magnitude below that of the numerical experiment. At intermediate scales, we also obtain the production of vorticity pairs behind the collision of strong shocks, but the intensity of the vortices is strongly reduced from the values that occur in the original calculation because of scaling effects.

We are now in the process of applying the hyperviscosity method described here to several problems. In particular, we plan to investigate the temporal variation of

the fluctuating Mach number with time at high Reynolds number for three-dimensional flows. We are also looking at the characteristic scale of shocks that emerges when varying the spatial scale of the initial conditions.

When dealing with the problem of star formation in a molecular cloud, self-gravity must be added to the fluid equations. The condensations that occur lead to cavitation which is difficult to handle numerically, since schemes do not in general preserve the positivity of the density. In that case, in addition to hyperviscosity to enhance the Reynolds number, one may add a mass diffusion term in the continuity equation that smooths out steep density gradients.

Finally, we would like to point out that nothing in principle impedes the usage of powers of the derivative fields higher than those tested here. However, with an explicit temporal numerical scheme, this would prove hard to handle and we have made no attempt to do so.

Appendix

We give here a brief description of the numerical method used in this paper. Our codes are pseudo-spectral, with space derivatives computed in spectral space and non-linear products in configuration space. The exchange between the two spaces is performed through a fast Fourier transform algorithm, written in machine language for the CRAY 1 by C. Temperton, in order to accelerate computations. The temporal scheme is second-order Adams–Bashforth. Having in mind the simulation of homogeneous flows at high Reynolds numbers, we choose periodic boundary conditions and write all variable fields as a Fourier series truncated at wavenumber $N_{\max}$.

To adapt the code to the CRAY 1S of the CCVR which has a relatively small memory and yet is a fast machine, we chose to minimize the number or arrays stored at the cost of extra FFT. At present, the code takes 14 $N_{\max} \times N_{\max}$ arrays of storage and requires the computation of 19 FFT for the two-dimensional fluid equations (2.1) written for a perfect gas in a conservative way. The maximum resolution we use is $N_{\max} = 256$, which takes 1.2 Mword of memory. This is achieved by transferring data to and from the central core and the peripheral memory: a time step at that resolution takes 0.6 s of CPU on the CRAY 1S and a typical run takes on the order of 3 h.

The choice of $N_{\max}$ in turn determines the Reynolds number that will be achieved in the simulation. It is adjusted in a dichotomous way, having to fulfil at least two conditions: the inertial range in which nonlinear mode coupling prevails be as wide as possible, but on the other hand, the energy spectrum in the large wavenumber range falls off sufficiently rapidly (no energy accumulation in the dissipative range). The limitation on the Reynolds numbers reasonably achieved on present-day computers for three-dimensional complex problems (such as those occurring in weather prediction for example) is drastic and the cost prohibitive, hence the search for adequate models of the small-scale flows.

ACKNOWLEDGMENTS

We use the FFT algorithm written by C. Temperton and the graphical software of NCAR. Computations have been performed on the CRAY 1 of the Centre de Calcul Vectoriel pour la Recherche under Contracts 1630 and 3674. This work received financial support from the CNRS through the RCP "Fluides Astrophysiques en Régime Supersonique" under Contract 080702 and the ATP "Dynamique des Fluides Astrophysiques et Géophysiques" under Contract 1227.

REFERENCES

1. J. LÉORAT, A. POUQUET, AND J.-P. POYET, in *Proceedings, Colloquium on Problems of Collapse and Numerical Relativity*, edited by M. Bancel and M. Signore (Reidel, Dordrecht, 1984), p. 287.
2. T. PASSOT AND A. POUQUET, "Expérimentation numérique sur la turbulence compressible à deux dimensions: le cas du gaz parfait," Proceedings, Colloque DRET-ONERA, Poitiers, Ecole Nationale Supérieure de Mécanique et d'Aérotechnique, 1986, p. 87.
3. T. PASSOT AND A. POUQUET, *J. Fluid Mech.* **181**, 441 (1987).
4. W. J. FEIEREISEN, W. C. REYNOLDS, AND J. H. FERZIGER, Report TF-13, Standard University, 1981 (unpublished).
5. R. B. LARSON, *Mon. Not. R. Astron. Soc.* **194**, 809 (1981).
6. P. J. ROACHE, *Computational Fluid Dynamics* (Hermosa, Albuquerque, NM, 1972).
7. P. WOODWARD AND P. COLELLA, *J. Comput. Phys.* **54**, 115 (1984).
8. O. A. LADYZHENSKAYA, *A Mathematical Theory of Viscous Incompressible Flows*, 1st ed., (Gordon & Breach, New York, 1963).
9. C. BASDEVANT, B. LEGRAS, R. SADOURNY, AND M. BÉLAND, *J. Atmos. Sci.* **38**, 2305 (1981).
10. J. C. MCWILLIAMS, *J. Fluid Mech.* **146**, 21 (1984).
11. M. MENEGUZZI, U. FRISCH, AND A. POUQUET, *Phys. Rev. Lett.* **47**, 1060 (1981).
12. D. GOTTLIEB AND S. A. ORSZAG, *Numerical Analysis of Spectral Methods* (Soc. Indus. Appl. Math., Philadelphia, 1977).
13. M. P. GERMAIN, Cours de Mécanique, Tome II (Ecole Polytechnique, Paris, 1982).
14. L. LANDAU AND E. LIFSHITZ, *Theory of Elasticity*, *Course of Theoretical Physics*, Vol. VII, Chap. 4 (Pergamon, London, 1967).
15. J. SMAGORINSKY, *Mon. Weather Rev.* **91**, 99 (1963).
16. H. HA MINH AND D. D. VANDROMME, Proceedings, DRET-ONERA Colloquium, Poitiers, Ecole Nationale Supérieure de Mécanique et Aérotechnique, 1986.